Dependence of heme biosynthesis on iron-sulfur cluster biogenesis: human ALAD is an unrecognized iron-sulfur protein

Gang Liu
National Institute of Child Health and Human Development
Debangsu Sil
Pennsylvania State University https://orcid.org/0000-0002-0718-3925
Wing-Hang Tong
National Institute of Child Health and Human Development, NIH
Nunziata Maio
National Institute of Child Health and Human Development
J. Martin Bollinger Jr.
The Pennsylvania State University
Carsten Krebs
Pennsylvania State University
Tracey Ann Rouault (rouault@mail.nih.gov)
National Institute of Child Health and Human Development https://orcid.org/0000-0003-0062-0245

Article

Keywords: ISC, iron-sulfur cluster, biogenesis, ALAD, heme biosynthesis

Posted Date: July 1st, 2020

DOI: https://doi.org/10.21203/rs.3.rs-37702/v1

Version of Record: A version of this preprint was published at Nature Communications on December 9th, 2020. See the published version at https://doi.org/10.1038/s41467-020-20145-9.

Abstract

Heme biosynthesis and iron-sulfur cluster (ISC) biogenesis are two major mammalian metabolic pathways that require iron. It has long been known that these two pathways interconnect, but the previously described interactions do not fully explain why heme biosynthesis depends on intact ISC biogenesis. Herein we have identified a previously unrecognized connection between these two pathways through our discovery that human aminolevulinic acid dehydratase (ALAD), which catalyzes the second step of heme biosynthesis, is an Fe-S protein. We found that several highly conserved cysteines and an Ala306-Phe307-Arg308 motif of human ALAD are important for [Fe_4S_4] cluster acquisition and coordination. The enzymatic activity of human ALAD was greatly reduced upon loss of its Fe-S cluster, which resulted in reduced heme biosynthesis in human cells. Our findings explain why heme biosynthesis depends on intact ISC biogenesis, as ALAD provides an early Fe-S-dependent checkpoint in the heme biosynthetic pathway.

Introduction

In mammalian cells, substantial amounts of iron are consumed by heme biosynthesis and iron-sulfur cluster (ISC) biogenesis[1, 2]. Heme is synthesized by eight sequential enzymatic steps[3], of which the first takes place in the mitochondrial matrix, where 5-aminolevulinate synthase (ALAS) catalyzes the condensation of succinyl-CoA with glycine to generate ALA (Figure S1)[3, 4]. Two *ALAS* genes are present in vertebrates, a ubiquitously expressed *ALAS1* and an erythroid-specific *ALAS2*[2, 5]. The mRNA of *ALAS2* has an iron responsive element (IRE) in its 5'-untranslated region (UTR) and is post-transcriptionally regulated by the iron regulatory proteins (IRP1 and IRP2)[6, 7]. Since IRP1 loses its IRE-binding activity when it ligates an Fe-S cluster, ALAS2 protein levels are indirectly regulated by ISC biogenesis because apo-IRP1 binding represses ALAS2 translation[6, 7]. ALAS1, which catalyzes the rate-limiting step of heme biosynthesis in non-erythroid cells[3], is subject to negative feedback regulation by cellular heme content[8, 9]. After its synthesis in mitochondria, ALA is exported to the cytosol, where ALA dehydratase (ALAD) catalyzes the second step of heme biosynthesis by condensing two ALA molecules into porphobilinogen (Figure S1). ALAD is evolutionarily conserved and constitutes an important enzyme for chlorophyll synthesis, the corrin ring of vitamin B12, and other important tetrapyrroles[10, 11]. After three additional enzymatic reactions in the cytosol and two in the mitochondria, the final insertion of ferrous iron into protoporphyrin IX to generate heme occurs in the mitochondrial matrix and is catalyzed by ferrochelatase (FECH) (Figure S1)[4]. Human FECH is an Fe-S protein[12, 13, 14], and its post-translational stability depends on coordination of a [Fe_2S_2] cluster[12, 15].

Iron-sulfur clusters are ancient prosthetic groups with essential biological functions[16, 17, 18, 19]. In the mitochondria of mammalian cells, ISCs are assembled de novo by a complex composed of NFS1, ISD11, ACP, the ISCU scaffold and frataxin[20]. After assembly, nascent clusters are transferred by an HSPA9/HSC20 chaperone/co-chaperone system directly to recipient proteins or through intermediate scaffolds[21]. Previous models have proposed that initial Fe-S synthesis occurs solely in the mitochondrial

matrix[22]. However, the core mammalian ISC components have also been identified in the cytosol and nucleus, and accumulating evidence shows that the ISC biogenesis machineries likely operate independently to generate nascent clusters in several subcellular compartments of multicellular eukaryotes[23, 24, 25]. We previously reported that binding of HSC20 to a leucine-tyrosine-arginine (LYR) motif of succinate dehydrogenase complex subunit B (SDHB) was essential for ISC incorporation into SDHB[26]. The LYR motif was also identified in other HSC20-binding proteins[26, 27]. Therefore, we speculated that analyzing protein sequences for the presence of the LYR motif and motifs with similar chemical properties (LYR-like motifs) could be used to discover candidate Fe-S proteins[26, 28].

Thus far, there are two well-characterized nodes in the heme biosynthetic pathway of mammalian cells at which defects in the Fe-S biogenesis machinery can suppress heme synthesis. First, FECH of higher eukaryotes contains a [Fe_2S_2] cluster that is proposed to stabilize the enzyme[12, 13]. Second, ALAS2 is post-transcriptionally regulated in erythroid cells by the interconversion of IRP1 between a holo-form that functions as cytosolic aconitase and an apo-IRE-binding protein that represses ALAS2 expression[7]. Therefore, Fe-S biogenesis defects can block heme synthesis by either repressing ALAS2 synthesis in erythroid cells or inactivating FECH. However, it remains unexplained how Fe-S biogenesis defects in yeast result in impaired heme production[29, 30], given that yeast FECH is not an Fe-S protein and yeast lack IRPs[12, 14]. The fact that Fe-S biogenesis deficiency impaired heme biosynthesis in yeast drove us to search for unrecognized intersections between the Fe-S and heme pathways using bioinformatics to screen heme biosynthetic enzymes for the presence of LYR motifs. We found that ALAD contained a LYR-like motif ($A_{306}F_{307}R_{308}$). Our previous extensive studies have revealed that the LYR-like motif can be defined as follows: position 1, a small amino acid with a more aliphatic character, including leucine, isoleucine, valine, alanine and a few others. The second position must be either Y or F (aromatic) and the third position must be either R or K (positively charged)[26, 28]. Here, we report that ALAD needs a [Fe_4S_4] cofactor for optimal enzymatic activity upon over-expression in human cells and in bacteria. We performed functional studies to elucidate the molecular mechanisms by which human ALAD acquires and coordinates the [Fe_4S_4] cluster, and to demonstrate the biological significance of the [Fe_4S_4] cluster.

Results

Human ALAD coordinates a previously unrecognized [Fe_4S_4] cluster

First, we explored whether there are as-yet-uncharacterized convergent points between the Fe-S and heme biosynthetic pathways. We first simultaneously knocked down the mitochondrial and cytosolic ISCU isoforms, which constitute the primary Fe-S biogenesis scaffolds in mammalian cells. Over-expression of yeast FECH, a non-Fe-S enzyme, did not restore heme biosynthesis in ISCU-deficient cells [Figures S2A-S2C and Supplemental Discussion (SD)]. Then we overexpressed a cytosolic ISCU mutant that impairs Fe-S biogenesis in the cytosol of mammalian cells and found that heme biosynthesis was inhibited (detailed in the SD and Figures S2D-S2F). Taken collectively, these results implied that one or more cytosolic heme biosynthetic steps was dependent on Fe-S biogenesis.

Then we screened the amino acid (AA) sequences of cytosolic heme biosynthesis enzymes for conserved LYR or LYR-like motifs to search for a potential Fe-S protein. Sequence alignment showed that human ALAD contains six cysteines, C119, C122, C124, C132, C162 and C223, and a LYR-like motif (Ala306-Phe307-Arg308) that is conserved among eukaryotic ALAD orthologs (Figure S3). Therefore, in terms of AA sequence and composition, ALAD appeared to represent a good candidate as an Fe-S protein.

As we have previously shown that de novo Fe-S biosynthesis occurs simultaneously in the mitochondrial and cytosolic compartments of mammalian cells[23], we first determined whether human ALAD interacted with cytosolic HSC20. When the cytosolic fraction of HeLa cells was immunoprecipitated with anti-HSC20 antibody, the eluate contained ALAD (Figure 1A), suggesting that endogenous cytosolic HSC20 (C-HSC20) interacted with ALAD. Because HSC20 binds directly to LYR motifs, permitting transfer of nascent clusters from ISCU directly to recipient proteins[16, 26], we then determined whether the AFR motif of human ALAD might be important for its interaction with HSC20. We transfected HeLa cells with plasmids expressing FLAG/MYC-tagged wild-type ALAD (ALAD WT) or AFR to alanine mutant (Mut AFR-AAA). Lysates from these cells were immunoprecipitated with anti-FLAG antibody, and the eluates were analyzed by western blotting. As shown in Figure 1B, wild-type ALAD interacted specifically with C-HSC20 but not with the lower-molecular-weight mitochondrial HSC20 (M-HSC20), as expected, given that ALAD is a cytosolic enzyme. No interaction between C-HSC20 and the AFR-AAA mutant was detected. Collectively, these data demonstrated that ALAD interacted with C-HSC20 and that the AFR motif of ALAD was important for the interaction.

To investigate whether human ALAD coordinates an ISC in human cells, we quantified ^{55}Fe incorporation into C-terminally FLAG/MYC-tagged POLD1 (POLD1), a known [Fe_4S_4] protein that acquires its cluster in the cytosol [31], C-terminally FLAG/MYC-tagged ALAD WT and C-terminally FLAG/MYC-tagged Mut AFR-AAA in HEK293 cells transfected with either a pool of non-targeting siRNAs (NT) or with si-RNAs directed against human *ISCU* (si-ISCU). We found that ALAD and POLD1 bound comparable amounts of ^{55}Fe in control HEK293 cells transfected with non-targeting siRNAs (Figure 1C and 1D). Mut AFR-AAA, which did not interact with C-HSC20 (Figure 1B), bound significantly less ^{55}Fe than ALAD WT in NT HEK293 cells (Figure 1C, $P<0.001$). Compared with control cells, ALAD and POLD1 bound significantly lower amounts of ^{55}Fe in HEK293 cells with defective ISC assembly machinery, achieved by silencing of human *ISCU* (Figure 1C and 1D, $P<0.001$). Taken together, these results demonstrated that ALAD binds iron, presumably in the form of an ISC, in human cells. To determine whether human ALAD can indeed coordinate an ISC in human cells, we then overexpressed C-terminally FLAG/MYC-tagged ALAD WT and Mut AFR-AAA in Expi293 cells and purified the recombinant proteins anaerobically. Anaerobically purified recombinant ALAD migrated as a single band on SDS-PAGE (Figure 1E) and exhibited a shoulder at ~420 nm in its UV-vis spectrum (Figure 1F), suggesting the presence of [Fe_4S_4] cluster(s)[32, 33, 34].

We next expressed N-terminally MBP-tagged human ALAD (MBP-ALAD) in growing bacteria along with the *A. vinelandii isc* operon, which encodes the basic Fe-S biogenesis proteins and can assist iron-sulfur cluster assembly in bacteria, and purified the expressed protein anaerobically[35, 36]. The anaerobically

purified MBP-ALAD was brown (Figure 1G), migrated as a single band on SDS-PAGE (Figure 1H), and also exhibited a shoulder at ~420 nm in its UV-vis spectrum (Figure 1I).

To validate the presence of $[Fe_4S_4]$ cluster(s) and determine the stoichiometry of the $[Fe_4S_4]$ cluster(s), a ^{57}Fe-enriched MBP-ALAD sample was analyzed by Mössbauer and EPR spectroscopies. The 4.2-K Mössbauer spectrum collected in a 0.53 mT magnetic field applied parallel to the direction of γ radiation (Figure 1J, black vertical bars) was dominated by a quadrupole doublet with parameters typical of $[Fe_4S_4]^{2+}$ clusters [isomer shift (δ) of 0.44 mm/s and quadrupole splitting parameter (ΔE_Q) of 1.24 mm/s, 79% of total intensity, red line][17, 37]. In addition, the spectrum revealed a small amount of another quadrupole doublet with typical $[Fe_2S_2]^{2+}$ parameters (δ = 0.28 mm/s and ΔE_Q = 0.50 mm/s, 11% of total intensity, blue line). Given that we measured that wild type ALAD binds 3.5 Fe per protein monomer (*vide infra*), the Mössbauer results imply that each ALAD monomer contains ~0.7 $[Fe_4S_4]^{2+}$ and ~0.2 $[Fe_2S_2]^{2+}$. $[Fe_2S_2]^{2+}$ clusters are known to form as a result of $[Fe_4S_4]^{2+}$ degradation[35]. Therefore, the minor quadrupole doublet corresponding to the $[Fe_2S_2]^{2+}$ cluster could be a result of breakdown of a fraction of relatively unstable $[Fe_4S_4]^{2+}$ clusters. Consistent with the Mössbauer analysis, the EPR spectrum showed no signal, ruling out the presence of Fe-S clusters with a half-integer spin ground state (i.e., $[Fe_2S_2]^{+}$, $[Fe_4S_4]^{+}$, $[Fe_4S_4]^{3+}$, $[Fe_3S_4]^{+}$) (Figure S4)[17, 37]. Taken together, these results demonstrate that each human ALAD monomer harbors one $[Fe_4S_4]$ cluster when it is expressed along with the *isc* operon and purified anaerobically.

$[Fe_4S_4]$-ALAD has significantly higher enzymatic activity than zinc-ALAD

ALAD was previously identified as a zinc enzyme, and structures with zinc in the active site have been studied[38, 39]. Therefore, to determine whether the $[Fe_4S_4]$ cluster of human ALAD is functionally significant, we compared the enzymatic activities of aerobically purified wild-type apo-ALAD (aero-apo-ALAD WT, see the Methods section for details), aerobically purified wild-type ALAD (aero-ALAD WT, aerobically purified wild-type ALAD prior to treating with EDTA,), aerobically purified wild-type zinc bound-ALAD (aero-Zn-ALAD WT), and the anaerobically purified wild-type ALAD. As demonstrated by the ICP-MS analysis, aero-apo-ALAD WT did not contain iron or zinc, while aero-ALAD WT contained no zinc and a small amount of iron (Figure 2A). The enzymatic activity of aero-Zn-ALAD WT was approximately six times and two times higher than those of aero-apo-ALAD WT and aero-ALAD WT, respectively (Figure 2A and 2B, P<0.01). These results suggested that the enzymatic activity of apo-ALAD can be partly restored by zinc reconstitution. Wild-type ALAD expressed along with *isc* operon and purified anaerobically (ALAD WT) did not contain zinc (Figure 2A). Its enzymatic activity was approximately three times higher than that of aero-Zn-ALAD WT (Figure 2B the third bar versus the second bar, P<0.01). These results demonstrate that $[Fe_4S_4]$-ALAD has significantly higher enzymatic activity than zinc-ALAD.

The six highly conserved cysteines, Lysine 252, and the LYR motif of human ALAD are important for the enzymatic activity of human ALAD that contains a $[Fe_4S_4]$ cluster *in vitro*

To identify the AAs important for the coordination/acquisition of the [Fe_4S_4], we mutagenized each of the six highly conserved cysteines, and Lys252, which has been shown to form a Schiff base with the carbonyl of one of the two ALA substrates in the enzymatic active site pocket (Figures S5 and S6). Additionally, we mutagenized the LYR-like motif of human ALAD to generate eight MBP-ALAD mutants (C119A, C122A, C124A, C132A, C162A, C223A, K252M, and Mut AFR-AAA). We expressed these mutants along with the bacterial *isc* operon and purified the over-expressed proteins anaerobically. To investigate whether the mutants coordinated a [Fe_4S_4] cluster, we plotted their molar extinction coefficients based on their UV-vis spectra. As shown in Figure 2C, none of UV-vis spectra of the mutants exhibited the absorption at ~420 nm, which is a hallmark feature of [Fe_4S_4] clusters. This observation indicates that these AAs are involved in either [Fe_4S_4] cluster coordination/acquisition or in maintaining the ALAD protein structure conducive to [Fe_4S_4] cluster coordination/acquisition. Importantly, the ALAD mutants all had significantly less iron and lower (or undetectable) enzymatic activities than ALAD WT (Figures 2A and 2B, *P* values <0.01). These results further confirm that the cysteines and LYR motif are important for [Fe_4S_4] cluster coordination/acquisition and the [Fe_4S_4] cluster is important for human ALAD enzymatic activity *in vitro*.

To determine whether the N-terminal MBP tag hindered the formation of a homo-octamer of ALAD subunits that constitute the previously defined active form of ALAD[40], and to assess how [Fe_4S_4] cluster coordination affected ALAD quaternary structure, the anaerobically purified wild-type and mutant ALAD proteins were subjected to native gel electrophoresis. As shown in Figure 2D, most of the ALAD WT monomers formed ~640 kD homo-octamers, while all the ALAD mutants and the aero-apo-ALAD WT mostly assembled into ~480 kD homo-hexamers, a previously identified less active multimeric enzyme[40]. These results suggested that MBP-ALAD can form homo-octamers *in vitro* and that [Fe_4S_4] cluster coordination correlated with formation of higher proportions of ALAD homo-octamers.

The [Fe_4S_4] cluster of human ALAD is crucial for its enzymatic activity and heme biosynthesis in HepG2 cells

Next, we investigated the biological significance of the [Fe_4S_4] cluster of ALAD in human HepG2 cells. We co-transfected HepG2 cells with siRNAs to knockdown (KD) the expression of endogenous ALAD, and with a plasmid directing expression of either recombinant wild type ALAD (the ALAD WT group) or the ALAD mutant in which the AFR motif had been replaced by alanines (Mut AFR-AAA group). Effective KD of endogenous ALAD was achieved in HepG2 cells (Figure 3A). Recombinant ALAD WT or the Mut AFR-AAA mutant were well expressed with undetectable background expression of endogenous ALAD (Figures 3A and 3B, *P* values <0.01). We used ALAS1 protein levels and the activities of the heme-dependent enzymes cytochrome P450 1A2 (CYP1A2) and catalase, as readouts of the integrity of the heme biosynthetic pathway[41, 42, 43]. As shown in Figures 3A, 3D and 3E, there were no significant differences in the protein level of ALAS1 and catalase and CYP1A2 activities between the ALAD WT group and untransfected HepG2 cells. In cells expressing ALAD-Mut AFR-AAA, however, we observed significantly decreased ALAD, catalase and CYP1A2 activities in cell lysates as compared with untransfected HepG2

cells and with cells expressing ALAD WT (Figures 3A and 3C-3E, *P* values <0.01). These results demonstrated that the AFR-AAA mutant was non-functional and exhibited significantly lower enzymatic activity than wild-type ALAD. Therefore, overexpression of ALAD-Mut AFR-AAA did not restore heme biosynthesis that was suppressed by siRNA-induced ALAD deficiency. Given that the AFR motif of human ALAD is required for [Fe_4S_4] cluster acquisition, these results demonstrate that the [Fe_4S_4] of human ALAD is important for its enzymatic activity and heme biosynthesis in HepG2 cells.

Finally, we examined whether zinc addition affected ALAD enzymatic activity by adding zinc to the medium of mammalian cells over-expressing either WT ALAD or the Mut AFR-AAA (100 μM $ZnCl_2$ for 48 hours). As shown in Figure 3A, levels of human metallothionein MT2A, whose expression is regulated by zinc[44, 45], were greatly increased, suggesting that levels of cellular zinc indeed increased. However, there were no significant changes in either the protein levels of ALAS1 or the activities of ALAD, catalase or CYP1A2 after adding $ZnCl_2$ to the medium (Figures 3A and 3C-3E). These results indicated that increasing intracellular zinc concentrations did not increase ALAD enzymatic activity in HepG2 cells overexpressing either wild-type ALAD or the AFR-AAA mutant. Notably, FECH protein levels were not affected by zinc addition, indicating that the coordination of [Fe_2S_2] cluster by human FECH was also unaffected by increased intracellular zinc levels (Figure 3A).

Discussion

In this study, we found that human ALAD requires a [Fe_4S_4] cluster to acquire its full enzymatic activity both *in vitro* and in HepG2 cells. More importantly, the [Fe_4S_4] cluster of ALAD is crucial for heme biosynthesis, unveiling a node of regulation of heme biosynthesis by ISC biogenesis that operates at the second step of the heme biosynthetic pathway.

To determine whether one or more steps of the cytosolic reactions of heme biosynthesis depended on Fe-S cluster biogenesis, we overexpressed a form of cytosolic ISCU that lacked a mitochondrial targeting signal and contained the mutation D46A, which prevents the ISCU scaffold from transferring its Fe-S cluster to recipient proteins in mammalian cells. Our results demonstrated that two heme-dependent enzymes, catalase and cytochrome P450 oxidase, lost activity when the D46A ISCU construct was expressed to suppress cytosolic Fe-S biogenesis. We then used bioinformatics to evaluate whether the AA sequences of any of the cytosolic heme biosynthesis enzymes contained LYR-like motifs and potential cluster-ligating cysteines, which we have shown may represent features of candidate Fe-S proteins[28]. Only human ALAD was found to contain an LYR-like motif, consisting of Ala306-Phe307-Arg308. ALAD had been previously characterized as a zinc protein, as ALAD purified from beef liver contained much larger amounts of zinc than iron[46]. Also, the low enzymatic activity of metal-free ALAD could be partially restored by zinc addition[46, 47]. In later studies, it was demonstrated that ALAD octamers required four zinc ions for enzymatic activity[38]. However, all these studies were performed under aerobic conditions that can interfere with identification of iron-sulfur clusters. In fact, many Fe-S proteins have been previously mischaracterized as zinc proteins, such as CPSF30[48], human CISD2[49], and yeast POL3[31]. Therefore, we

decided to explore whether ALAD is an Fe-S protein. According to our results, human ALAD can coordinate an ISC in human cells. In addition, each human ALAD monomer harbored one [Fe_4S_4] cluster when it was expressed along with the *isc* operon and purified anaerobically.

We then compared the enzymatic activity of [Fe_4S_4]-ALAD with that of zinc-ALAD and found that [Fe_4S_4]-ALAD had significantly higher enzymatic activity than zinc-ALAD. ALAD catalyzes the asymmetric condensation of two ALA molecules to form porphobilinogen. The ALA molecule that becomes the propionyl side chain and pyrrole nitrogen-containing part of porphobilinogen is named P-side ALA, whereas that which contributes the acetyl side chain and amino nitrogen-containing part of porphobilinogen is known as the A-side ALA. According to previous studies, the first step of this enzymatic reaction is the formation of P-side Schiff base of ALA with the nitrogen of lysine 252, followed by A-side ALA binding to the other side of enzymatic active site pocket[47, 50, 51, 52, 53]. It was proposed that in zinc-ALAD, the zinc functioned as a Lewis acid to bind A-side ALA[51]. Based on the resemblance of the ALAD reaction to those catalyzed by aconitase[54], dihydroxyacid dehydratase[55], and quinolinate synthase[56,58], we speculate that the [Fe_4S_4] cluster of ALAD is coordinated by only three Cys ligands, and the non-Cys-coordinated iron may function as a Lewis acid and may be coordinated by the ALA substrate, thereby enabling dehydration to take place (Figure S5)[54, 57]. As a [Fe_4S_4] cluster occupies a larger space than Zn(II), we further speculate that the [Fe_4S_4] cluster of ALAD forces the A-side ALA to move closer to the P-side ALA than when ALA is bound to Zn(II), thereby optimizing proximity of the two ALA molecules and facilitating the condensation reaction.

Most Fe-S proteins coordinate their clusters through cysteines[17, 58]. To identify the cysteines important for [Fe_4S_4] cluster acquisition and/or coordination, we mutagenized the six highly conserved cysteines of human ALAD to alanine residues (A). According to previous studies, lysines 210 (K210) and 263 (K263) in yeast ALAD, which correspond to K199 and K252 in human ALAD, form Schiff bases with two molecules of ALA to facilitate their condensation[59, 60]. Therefore, we also mutagenized K252 in human ALAD to methionine to investigate the impact of a K252M mutant on [Fe_4S_4] cluster coordination and ALAD enzymatic activity. To examine the biological significance of the AFR motif, we substituted it with three alanines (Mut AFR-AAA). According to our results, all the AA residues investigated are important for [Fe_4S_4] cluster coordination and the enzymatic activity of human ALAD *in vitro*. Our findings are consistent with those of a previous study in which a combination of C122A, C124A and C132A greatly reduced activity of human ALAD that ligates zinc[38]. In both the zinc-containing form of the enzyme which can be generated *in vitro*, and the Fe-S-containing form detected after overexpression in bacteria, cysteines 122, 124 and 132 appear to be required for acquisition of enzymatic activity. Consistent with these findings, a Cys132Arg mutation was found to be responsible for ALAD porphyria in a 14-year-old boy[61]. Furthermore, we speculate that the structure of ALAD with a [Fe_4S_4] cluster may resemble the crystal structure of Zn-ALAD (Figure S6)[39], and Cys residues 122, 124, and 132, the Zn(II) ligands in the published structures of ALAD[39], might coordinate the [Fe_4S_4] cofactor, of which the unique, non-Cys-coordinated Fe site can be coordinated by the ALA substrate[54, 57, 62]. Cys119 and Cys162 are located on

two parallel beta-strands (Figure S6) in positions where they have been proposed to form a disulfide bond that stabilizes ALAD tertiary structure[38]. Therefore, mutagenesis of the cysteine residues that ligate zinc in the available crystal structure may directly affect ISC ligation, whereas mutagenesis of C119 and C162 can impair cluster ligation as a result of misfolding of ALAD. Note that the K252M mutant completely lost its enzymatic activity. We speculate that this may be caused by loss of binding of one of the two ALA molecules that are condensed to form porphobilinogen in the “active site pocket” as previously defined[59, 60], but Fe-S ligation was notably absent as well for unclear reasons.

The quaternary structure of human ALAD can switch between a homo-hexameric and a homo-octameric configuration[40]. Wild-type ALAD monomers tend to form a homo-octamer with full enzymatic activity through interactions between their N-terminal domains[40, 63]. In the presence of *ALAD* mutations or of “morphlocks”, small molecules that stabilize specific quaternary structures, ALAD can assemble into a homo-hexameric configuration with lower enzymatic activity than the homo-octameric configuration[63, 64]. In this study, we found that [Fe_4S_4] cluster coordination correlated with increased proportions of ALAD homo-octamers, which may be another reason why [Fe_4S_4]-ALAD has high enzymatic activity.

Finally, we explored the biological significance of the [Fe_4S_4] cluster of ALAD in human HepG2 cells. We performed functional assays to investigate whether overexpression of either wild-type human ALAD or the AFR-AAA mutant could rescue the heme biosynthetic defect of ALAD-knockdown cells. According to our results, the [Fe_4S_4] of human ALAD is important for its enzymatic activity and heme biosynthesis in HepG2 cells. Interestingly, we also found that increased intracellular zinc concentrations, achieved by adding $ZnCl_2$ into the cell culture medium, did not increase ALAD enzymatic activity in wild-type ALAD- or AFR-AAA mutant-overexpressing HepG2 cells, suggesting that mammalian cells lack mechanisms that specifically deliver zinc to ALAD in growing cells.

In conclusion, our findings have several important biological implications. In iron-deficient non-erythroid cells, reduced ISC availability will decrease the enzymatic activity of ALAD, diminishing the potential accumulation of pyrroles and porphyrins synthesized downstream of ALAD that could otherwise occur in conjunction with reduced holo-FECH levels and/or increased ALAS1 protein levels. Porphyrin intermediates are toxic, and their accumulation causes several types of human porphyria[65, 66, 67]. Therefore, the regulation of ALAD activity by ISC biogenesis may represent a new mechanism preventing iron- or ISC-deficient non-erythroid cells from building up harmful heme metabolic intermediates. In addition, given that Fe-S clusters are sensitive to oxidative stress and that ALAD was shown to be a direct target of oxidative stress[17, 68], we speculate that oxidative damage of the [Fe_4S_4] of human ALAD may be implicated in pathological conditions associated with both increased oxidative stress and anemia, such as chronic renal failure[69]. Furthermore, since we confirmed the biological significance of a LYR or LYR-like motif, our study validates our prediction that enzymes unrelated to the mitochondrial respiratory chain depend on Fe-S delivery from a co-chaperone/chaperone pathway that is critical for Fe-S acquisition[26]. Our work may encourage researchers to identify other novel Fe-S proteins based on presence of LYR

motifs in proteins that contain cysteine ligands for Fe-S coordination in an adjacent peptide or protein complex.

Methods

All the data in this study are available upon request.

Cell culturing and transfection

Human cervical carcinoma HeLa cells, HEK293 cells, and hepatocellular carcinoma HepG2 cells were obtained from ATCC. Expi293 cells were purchased from ThermoFisher Scientific. The stably-transfected HEK293T cell lines were established in our previous study[23]. All cell lines were subjected to mycoplasma testing. Detailed information about cell culturing is provided in the Supplemental Document (SD). Transient transfections were performed using the Lipofectamine® 2000 (Invitrogen) and Lipofectamine® RNAiMAX Reagent (Invitrogen). See SD for detailed transfection and zinc treatment procedures.

Cell fractionation and anaerobic purification of recombinant wild-type and mutant ALAD from mammalian cells

Organelle and cytosolic fractions were separated with the Mitochondria Isolation Kit (ThermoFisher) according to the manufacturer's protocol.

Immunoprecipitations of recombinant FLAG/MYC-tagged POLD1 (POLD1), wild-type ALAD (ALAD WT), or ALAD mutant of the AFR motif (Mut AFR-AAA) were performed on cytosolic fractions from HEK293 or Expi293 cells in a nitrogen recirculated glove box operated at <0.2 ppm O_2 48h after transfection with plasmids encoding POLD1, ALAD WT, or Mut AFR-AAA. Anti-FLAG immunoprecipitations were performed using M2-FLAG beads (Sigma). Washed FLAG M2 beads were added to the lysate and incubated for 2 h at room temperature under mild agitation. After the beads were recovered, recombinant proteins were competitively eluted with 100 µg/ml 3xFLAG peptide (Sigma).

UV-vis spectra were acquired using a NanoDrop spectrophotometer (ThermoFisher) using a column buffer supplemented with 100 µg/ml 3xFLAG peptide as the blank.

^{55}Fe incorporation assay

HEK293 cells were grown in the presence of 1 µM 55Fe-Tf and transfected twice at 48h interval with si-RNAs targeting ISCU or with non-targeting si-RNAs. At the time of the second transfection with si-RNAs, cells were co-transfected with FLAG/Myc-tagged ALAD WT or Mut AFR-AAA, or with FLAG/Myc-tagged POLD1, which was included in the experiment as a positive control. Cytosolic extracts were prepared in the glove box after the second transfection and subjected to immunoprecipitation with anti-FLAG M2 agarose beads.

^{55}Fe incorporation into recombinant proteins was measured by scintillation counting of FLAG-beads after immunoabsorption of FLAG-tagged recombinant proteins, followed by extensive washings with buffer I [25 mM Tris, 0.15 M NaCl, 1 mM EDTA, 1% NP-40, 5% glycerol (pH 7.4), protease and phosphatase inhibitor cocktail with no EDTA (Roche)]. The background, corresponding to ^{55}Fe measurements of eluates after anti-FLAG immunoprecipitations on cytosolic extracts from cells transfected with the empty vector (pCMV6-Entry; Origene), was subtracted from each reading.

Overexpression and anaerobic purification of maltose-binding protein (MBP)-tagged human ALAD proteins

BL21(DE3) competent bacterial cells (NEB) were co-transformed with pDB1282, a plasmid directing expression of *Azotobacter vinelandii isc* operon, and pMALc5x-MBP-ALAD plasmids, which directs expression of N-terminally MBP-tagged wild-type or mutant human ALAD proteins. The co-transformants were then cultured, induced for protein expression and lysed anaerobically. The N-terminally MBP-tagged ALAD proteins were then purified by affinity chromatography. See SD for details.

Ultraviolet-visible (UV-vis) spectroscopy, inductively coupled plasma mass spectrometry (ICP-MS), amino acid analysis (AAA), electron paramagnetic resonance (EPR) spectroscopy and Mössbauer spectroscopy

Uv-vis spectra were acquired using a NanoDrop spectrophotometer (ThermoFisher) with column buffer supplemented with 10 mM maltose used as the blank. For ICP-MS, 25 µL sample was digested overnight and iron and zinc concentrations were determined with an Agilent 7900 ICP-MS system. AAA was performed by Alphalyse to precisely quantify the purified ALAD proteins. To verify the presence of an iron-sulfur cluster, the anaerobically purified MBP-ALAD (250 µM) was subjected to both EPR and Mössbauer analyses. See SD for details.

Preparation of apo-ALAD and zinc-bound ALAD

Aerobically purified human ALAD was treated with 10 mM EDTA for 1 h and passed through a G-25 column (GE Healthcare) to yield metal-free ALAD (apo-ALAD). For zinc reconstitution, apo-ALAD was incubated with 5 mM dithiothreitol and 20 equivalents of $ZnCl_2$ at room temperature for 2 h and subsequently passed through a G-25 column.

Western blotting, co-immunoprecipitation and native gel electrophoresis

Organelle and cytosolic fractions were lysed with M-PER® Protein Extraction Reagent (ThermoFisher). For western blotting, 20-40 µg protein sample was used. Mouse monoclonal anti-FLAG antibody was from Origene, anti-ISCU rabbit polyclonal serum was raised against a synthetic peptide fragment, as previously reported[25]; anti α-TUB antibody was from Sigma. All the other primary antibodies for western blotting were from Abcam.

Co-immunoprecipitation (Co-IP) was carried out using the Pierce Co-Immunoprecipitation Kit (ThermoFisher). See SD for details.

For native gel electrophoresis, anaerobically purified ALAD proteins were separated, and the bands were visualized using the NativePAGE™ Bis-Tris Gel System (ThermoFisher) according to the manufacturer's instructions.

ALAD, cytochrome P450 (CYP), and catalase activity assays

ALAD activity was determined according to a published protocol[70]. The CYP and catalase activities were analyzed by the CYP1A2 Activity Assay Kit (Abcam) and Catalase Activity Assay Kit (Abcam), respectively.

Statistical analysis

Where applicable, three independent replicates were performed, and results are presented as mean ± standard deviation (S.D.). Two-sided Student's *t*-test was used to determine the *P* value. $P<0.05$ and $P<0.01$ were considered significant (* or ^{a}) and very significant (** or ^{aa}), respectively. Statistical analyses of ^{55}Fe labeling experiments were performed with GraphPad Prism 7 using two-way analysis of variance (ANOVA).

Declarations

Author Contributions

G.L. designed and performed the experiments, analyzed the data and wrote the manuscript. D.S. performed the Mössbauer and EPR experiments, analyzed the data and wrote the manuscript. W.T. and M.N. designed the experiments and analyzed the data. J.M.B and C.K. analyzed the Mössbauer and EPR data. T.A.R. designed and supervised the study, analyzed the data and wrote the manuscript. All authors revised the article critically.

Acknowledgements

We are grateful to all the members of our lab for constructive discussions and to Dr. Gregory Holmes-Hampton for his help on ICP-MS analysis. This work was supported by the Intramural Program of the *Eunice Kennedy Shriver* National Institute of Child Health and Human Development and the National Institutes of Health (GM-127079 to C.K.).

References

1. Muckenthaler MU, Rivella S, Hentze MW, Galy B. A Red Carpet for Iron Metabolism. *Cell* **168**, 344-361 (2017).

2. Kafina MD, Paw BH. Intracellular iron and heme trafficking and metabolism in developing erythroblasts. *Metallomics* **9**, 1193-1203 (2017).
3. Ponka P. Tissue-specific regulation of iron metabolism and heme synthesis: distinct control mechanisms in erythroid cells. *Blood* **89**, 1-25 (1997).
4. Ajioka RS, Phillips JD, Kushner JP. Biosynthesis of heme in mammals. *Biochim Biophys Acta* **1763**, 723-736 (2006).
5. Schultz IJ, Chen CY, Paw BH, Hamza I. Iron and Porphyrin Trafficking in Heme Biogenesis. *J Biol Chem* **285**, 26753-26759 (2010).
6. Rouault TA, Maio N. Biogenesis and functions of mammalian iron-sulfur proteins in the regulation of iron homeostasis and pivotal metabolic pathways. *J Biol Chem* **292**, 12744-12753 (2017).
7. Ye H*, et al.* Glutaredoxin 5 deficiency causes sideroblastic anemia by specifically impairing heme biosynthesis and depleting cytosolic iron in human erythroblasts. *J Clin Invest* **120**, 1749-1761 (2010).
8. Kubota Y, Nomura K, Katoh Y, Yamashita R, Kaneko K, Furuyama K. Novel Mechanisms for Heme-dependent Degradation of ALAS1 Protein as a Component of Negative Feedback Regulation of Heme Biosynthesis. *J Biol Chem* **291**, 20516-20529 (2016).
9. Zheng J, Shan Y, Lambrecht RW, Donohue SE, Bonkovsky HL. Differential regulation of human ALAS1 mRNA and protein levels by heme and cobalt protoporphyrin. *Mol Cell Biochem* **319**, 153-161 (2008).
10. Jaffe EK. The porphobilinogen synthase family of metalloenzymes. *Acta Crystallogr D Biol Crystallogr* **56**, 115-128 (2000).
11. Battersby AR. Tetrapyrroles: the pigments of life. *Nat Prod Rep* **17**, 507-526 (2000).
12. Dailey HA, Finnegan MG, Johnson MK. Human Ferrochelatase Is an Iron-Sulfur Protein. *Biochemistry* **33**, 403-407 (1994).
13. Wu CK, Dailey HA, Rose JP, Burden A, Sellers VM, Wang BC. The 2.0 A structure of human ferrochelatase, the terminal enzyme of heme biosynthesis. *Nat Struct Biol* **8**, 156-160 (2001).
14. Dailey HA*, et al.* Ferrochelatase at the millennium: structures, mechanisms and [2Fe-2S] clusters. *Cell Mol Life Sci* **57**, 1909-1926 (2000).
15. Crooks DR, Ghosh MC, Haller RG, Tong WH, Rouault TA. Posttranslational stability of the heme biosynthetic enzyme ferrochelatase is dependent on iron availability and intact iron-sulfur cluster assembly machinery. *Blood* **115**, 860-869 (2010).
16. Maio N, Rouault TA. Iron-sulfur cluster biogenesis in mammalian cells: New insights into the molecular mechanisms of cluster delivery. *BBA-Mol Cell Res* **1853**, 1493-1512 (2015).
17. Beinert H, Holm RH, Munck E. Iron-sulfur clusters: Nature's modular, multipurpose structures. *Science* **277**, 653-659 (1997).
18. Broderick JB, Duffus BR, Duschene KS, Shepard EM. Radical S-Adenosylmethionine Enzymes. *Chem Rev* **114**, 4229-4317 (2014).

19. Booker SJ. Anaerobic functionalization of unactivated C-H bonds. *Curr Opin Chem Biol* **13**, 58-73 (2009).
20. Rouault TA. The indispensable role of mammalian iron sulfur proteins in function and regulation of multiple diverse metabolic pathways. *Biometals* **32**, 343-353 (2019).
21. Rouault TA. Biogenesis of iron-sulfur clusters in mammalian cells: new insights and relevance to human disease. *Dis Model Mech* **5**, 155-164 (2012).
22. Braymer JJ, Lill R. Iron-sulfur cluster biogenesis and trafficking in mitochondria. *J Biol Chem* **292**, 12754-12763 (2017).
23. Kim KS, Maio N, Singh A, Rouault TA. Cytosolic HSC20 integrates de novo iron-sulfur cluster biogenesis with the CIAO1-mediated transfer to recipients. *Hum Mol Genet* **27**, 837-852 (2018).
24. Tong WH, Rouault T. Distinct iron-sulfur cluster assembly complexes exist in the cytosol and mitochondria of human cells. *EMBO J* **19**, 5692-5700 (2000).
25. Tong WH, Rouault TA. Functions of mitochondrial ISCU and cytosolic ISCU in mammalian iron-sulfur cluster biogenesis and iron homeostasis. *Cell Metab* **3**, 199-210 (2006).
26. Maio N, Singh A, Uhrigshardt H, Saxena N, Tong WH, Rouault TA. Cochaperone Binding to LYR Motifs Confers Specificity of Iron Sulfur Cluster Delivery. *Cell Metab* **19**, 445-457 (2014).
27. Maio N, Kim KS, Singh A, Rouault TA. A Single Adaptable Cochaperone-Scaffold Complex Delivers Nascent Iron-Sulfur Clusters to Mammalian Respiratory Chain Complexes I-III. *Cell Metab* **25**, 945-953 e946 (2017).
28. Rouault TA. Iron-sulfur proteins hiding in plain sight. *Nat Chem Biol* **11**, 442-445 (2015).
29. Lesuisse E, Santos R, Matzanke BF, Knight SA, Camadro JM, Dancis A. Iron use for haeme synthesis is under control of the yeast frataxin homologue (Yfh1). *Hum Mol Genet* **12**, 879-889 (2003).
30. Santos R, Buisson N, Knight SA, Dancis A, Camadro JM, Lesuisse E. Candida albicans lacking the frataxin homologue: a relevant yeast model for studying the role of frataxin. *Mol Microbiol* **54**, 507-519 (2004).
31. Netz DJ*, et al.* Eukaryotic DNA polymerases require an iron-sulfur cluster for the formation of active complexes. *Nat Chem Biol* **8**, 125-132 (2011).
32. Tong WH, Jameson GN, Huynh BH, Rouault TA. Subcellular compartmentalization of human Nfu, an iron-sulfur cluster scaffold protein, and its ability to assemble a [4Fe-4S] cluster. *Proc Natl Acad Sci U S A* **100**, 9762-9767 (2003).
33. Duin EC*, et al.* [2Fe-2S] to [4Fe-4S] cluster conversion in Escherichia coli biotin synthase. *Biochemistry* **36**, 11811-11820 (1997).
34. Arragain S*, et al.* Nonredox thiolation in tRNA occurring via sulfur activation by a [4Fe-4S] cluster. *Proc Natl Acad Sci U S A* **114**, 7355-7360 (2017).
35. Lanz ND, Grove TL, Gogonea CB, Lee K-H, Krebs C, Booker SJ. RlmN and AtsB as models for the overproduction and characterization of radical SAM proteins. In: *Method Enzymol*). Elsevier (2012).

36. Johnson DC, Unciuleac MC, Dean DR. Controlled expression and functional analysis of iron-sulfur cluster biosynthetic components within Azotobacter vinelandii. *J Bacteriol* **188**, 7551-7561 (2006).
37. Pandelia ME, Lanz ND, Booker SJ, Krebs C. Mossbauer spectroscopy of Fe/S proteins. *BBA-Mol Cell Res* **1853**, 1395-1405 (2015).
38. Jaffe EK, Martins J, Li J, Kervinen J, Dunbrack RL. The molecular mechanism of lead inhibition of human porphobilinogen synthase. *J Biol Chem* **276**, 1531-1537 (2001).
39. Mills-Davies N*, et al.* Structural studies of substrate and product complexes of 5-aminolaevulinic acid dehydratase from humans, Escherichia coli and the hyperthermophile Pyrobaculum calidifontis. *Acta Crystallogr D Biol Crystallogr* **73**, 9-21 (2017).
40. Jaffe EK. The porphobilinogen synthase family of metalloenzymes. *Acta Crystallogr D Biol Crystallogr* **56**, 115-128 (2000).
41. Correia MA, Sinclair PR, De Matteis F. Cytochrome P450 regulation: the interplay between its heme and apoprotein moieties in synthesis, assembly, repair, and disposal. *Drug Metab Rev* **43**, 1-26 (2011).
42. Sinclair PR, Gorman N, Jacobs JM. Measurement of heme concentration. *Curr Protoc Toxicol* **Chapter 8**, Unit 8 3 (2001).
43. Vlasits J, Jakopitsch C, Bernroitner M, Zamocky M, Furtmuller PG, Obinger C. Mechanisms of catalase activity of heme peroxidases. *Arch Biochem Biophys* **500**, 74-81 (2010).
44. Richards MP, Cousins RJ. Mammalian zinc homeostasis: requirement for RNA and metallothionein synthesis. *Biochem Biophys Res Commun* **64**, 1215-1223 (1975).
45. Davis SR, Cousins RJ. Metallothionein expression in animals: a physiological perspective on function. *J Nutr* **130**, 1085-1088 (2000).
46. Cheh A, Neilands JB. Zinc, an Essential Metal-Ion for Beef Liver Delta-Aminolevulinate Dehydratase. *Biochem Biophys Res Commun* **55**, 1060-1063 (1973).
47. Bevan DR, Bodlaender P, Shemin D. Mechanism of porphobilinogen synthase. Requirement of Zn2+ for enzyme activity. *J Biol Chem* **255**, 2030-2035 (1980).
48. Shimberg GD*, et al.* Cleavage and polyadenylation specificity factor 30: An RNA-binding zinc-finger protein with an unexpected 2Fe-2S cluster. *Proc Natl Acad Sci U S A* **113**, 4700-4705 (2016).
49. Conlan AR*, et al.* Crystal structure of Miner1: The redox-active 2Fe-2S protein causative in Wolfram Syndrome 2. *J Mol Biol* **392**, 143-153 (2009).
50. Jaffe EK, Hanes D. Dissection of the early steps in the porphobilinogen synthase catalyzed reaction. Requirements for Schiff's base formation. *J Biol Chem* **261**, 9348-9353 (1986).
51. Jaffe EK. The porphobilinogen synthase catalyzed reaction mechanism. *Bioorg Chem* **32**, 316-325 (2004).
52. Jaffe EK. The Remarkable Character of Porphobilinogen Synthase. *Acc Chem Res* **49**, 2509-2517 (2016).

53. Barnard GF, Itoh R, Hohberger LH, Shemin D. Mechanism of porphobilinogen synthase. Possible role of essential thiol groups. *J Biol Chem* **252**, 8965-8974 (1977).
54. Beinert H, Kennedy MC, Stout CD. Aconitase as iron-sulfur protein, enzyme, and iron-regulatory protein. *Chem Rev* **96**, 2335-2373 (1996).
55. Flint DH, Emptage MH, Finnegan MG, Fu WG, Johnson MK. The Role and Properties of the Iron-Sulfur Cluster in Escherichia-Coli Dihydroxy-Acid Dehydratase. *Journal of Biological Chemistry* **268**, 14732-14742 (1993).
56. Esakova OA, Silakov A, Grove TL, Warui DM, Yennawar NH, Booker SJ. An Unexpected Species Determined by X-ray Crystallography that May Represent an Intermediate in the Reaction Catalyzed by Quinolinate Synthase. *Journal of the American Chemical Society* **141**, 14142-14151 (2019).
57. Saunders AH*, et al.* Characterization of quinolinate synthases from Escherichia coli, Mycobacterium tuberculosis, and Pyrococcus horikoshii indicates that [4Fe-4S] clusters are common cofactors throughout this class of enzymes. *Biochemistry* **47**, 10999-11012 (2008).
58. Rouault TA. Mammalian iron-sulphur proteins: novel insights into biogenesis and function. *Nat Rev Mol Cell Biol* **16**, 45-55 (2015).
59. Rocha JBT, Saraiva RA, Garcia SC, Gravina FS, Nogueira CW. Aminolevulinate dehydratase (delta-ALA-D) as marker protein of intoxication with metals and other pro-oxidant situations. *Toxicol Res* **1**, 85-102 (2012).
60. Erskine PT*, et al.* X-ray structure of 5-aminolaevulinate dehydratase, a hybrid aldolase. *Nat Struct Biol* **4**, 1025-1031 (1997).
61. Akagi R, Kato N, Inoue R, Anderson KE, Jaffe EK, Sassa S. delta-Aminolevulinate dehydratase (ALAD) porphyria: the first case in North America with two novel ALAD mutations. *Mol Genet Metab* **87**, 329-336 (2006).
62. Flint DH, Allen RM. Iron-sulfur proteins with nonredox functions. *Chem Rev* **96**, 2315-2334 (1996).
63. Lawrence SH, Ramirez UD, Selwood T, Stith L, Jaffe EK. Allosteric Inhibition of Human Porphobilinogen Synthase. *J Biol Chem* **284**, 35807-35817 (2009).
64. Jaffe EK, Stith L. ALAD porphyria is a conformational disease. *Am J Hum Genet* **80**, 329-337 (2007).
65. Puy H, Gouya L, Deybach JC. Porphyrias. *Lancet* **375**, 924-937 (2010).
66. Cappellini MD, Brancaleoni V, Graziadei G, Tavazzi D, Di Pierro E. Porphyrias at a glance: diagnosis and treatment. *Intern Emerg Med* **5 Suppl 1**, S73-80 (2010).
67. Phillips JD. Heme biosynthesis and the porphyrias. *Mol Genet Metab*, (2019).
68. Goncalves TL, Benvegnu DM, Bonfanti G, Frediani AV, Pereira DV, Rocha JB. Oxidative stress and delta-ALA-D activity in different conditioning regimens in allogeneic bone marrow transplantation patients. *Clin Biochem* **42**, 602-610 (2009).
69. Eschbach JW. The anemia of chronic renal failure: pathophysiology and the effects of recombinant erythropoietin. *Kidney Int* **35**, 134-148 (1989).

70. Fujita H. Measurement of delta-aminolevulinate dehydratase activity. *Curr Protoc Toxicol* **Chapter 8**, Unit 8 6 (2001).

Figures

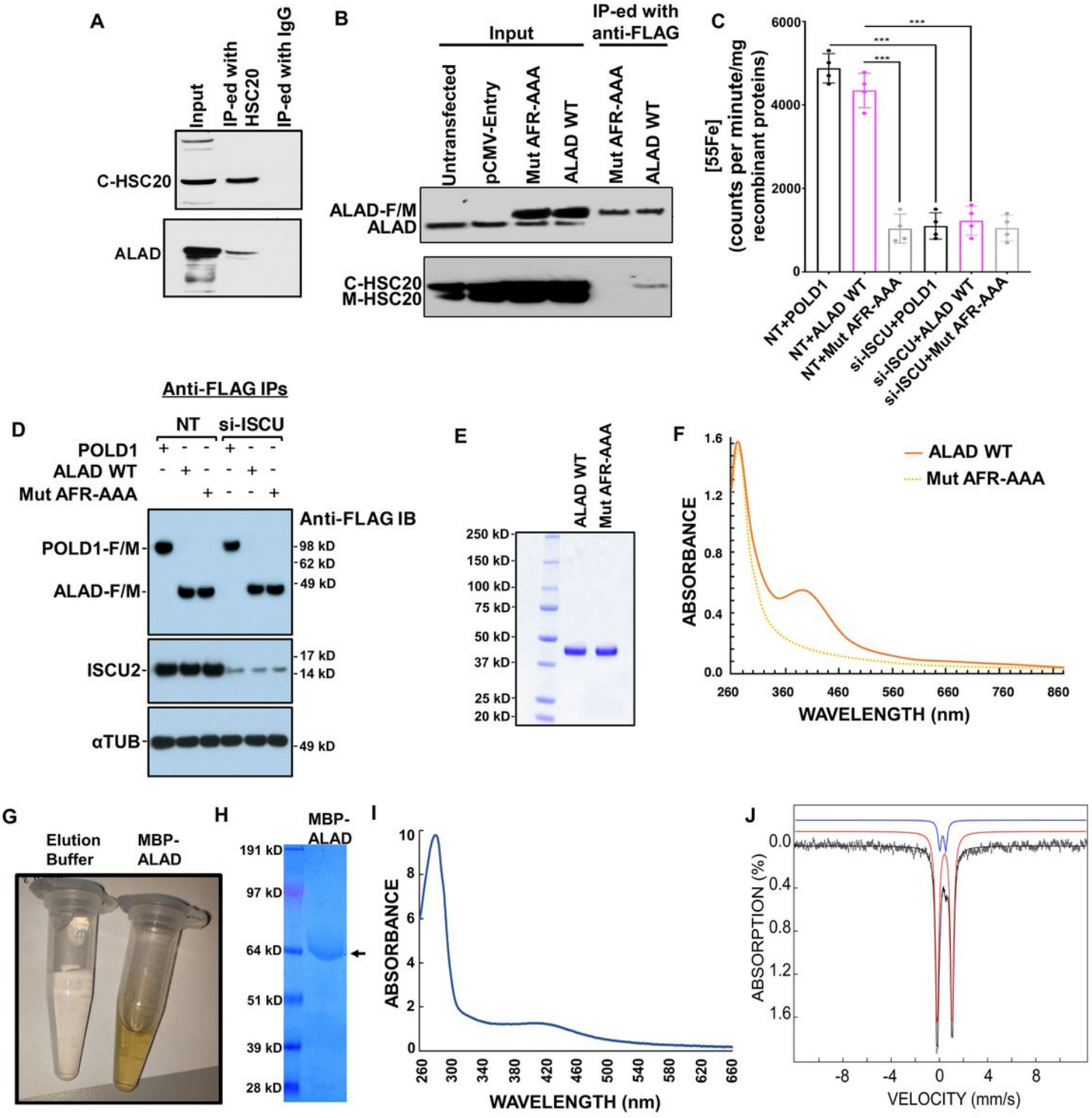

Figure 1

Human ALAD expressed in both human cells and bacteria (along with the isc operon) coordinates a [Fe4S4] cluster (A) Immunoprecipitation (IP) of cytosolic fractions of HeLa cells using anti-HSC20 antibody shows that ALAD co-precipitates with HSC20. The input was 5% of the cytosolic fraction lysate, and the remaining 95% of the lysate was subjected to IP with anti-HSC20 antibody. The eluates were then subjected to Western blotting with anti-HSC20 and anti-ALAD antibodies. (B) IP of whole cell lysates of HeLa cells transfected with plasmids expressing C-terminally FLAG/MYC-tagged wild-type ALAD (ALAD WT) or the AFR to AAA mutant (Mut AFR-AAA). The inputs were 10% of lysates used in the IPs. Untransfected HeLa cells or HeLa cells transfected with empty vector (pCMV-Entry) were used as controls. These results indicated that the AFR motif of human ALAD was important for its interaction with HSC20. (C) 55Fe incorporation into C-terminally FLAG/MYC-tagged POLD1 (POLD1), ALAD WT and Mut AFR-AAA in HEK293 cells transfected with non-targeting siRNA (NT) or On-TARGETPlus si-RNA pools against human ISCU (si-ISCU). (D) Immunoblot (IB) analysis of levels of the recombinant proteins subjected to 55Fe incorporation analysis in panel C. (E) Coomassie staining and (F) UV-vis spectra of C-terminally FLAG/MYC-tagged ALAD WT and Mut AFR-AAA that were expressed in Expi293 cells and purified anaerobically. (G) Photograph of elution buffer (left) and MBP-ALAD expressed along with isc operon in E. coli and purified anaerobically (right), which showed brown coloration of overexpressed holo-ALAD. (H) Coomassie staining of the anaerobically purified MBP-ALAD. (I) UV-vis spectrum of the anaerobically purified MBP-ALAD showing absorbance at 420 nm. (J) Experimental 4.2-K/53-mT Mössbauer spectrum of the anaerobically purified MBP-ALAD (black vertical bars) and simulation (black solid line) along with contributions from individual subspectra associated with [Fe4S4]2+ (red line) and [Fe2S2]2+ clusters (blue line) with parameters quoted in the text. Error bars represent S.D.; *** P<0.001.

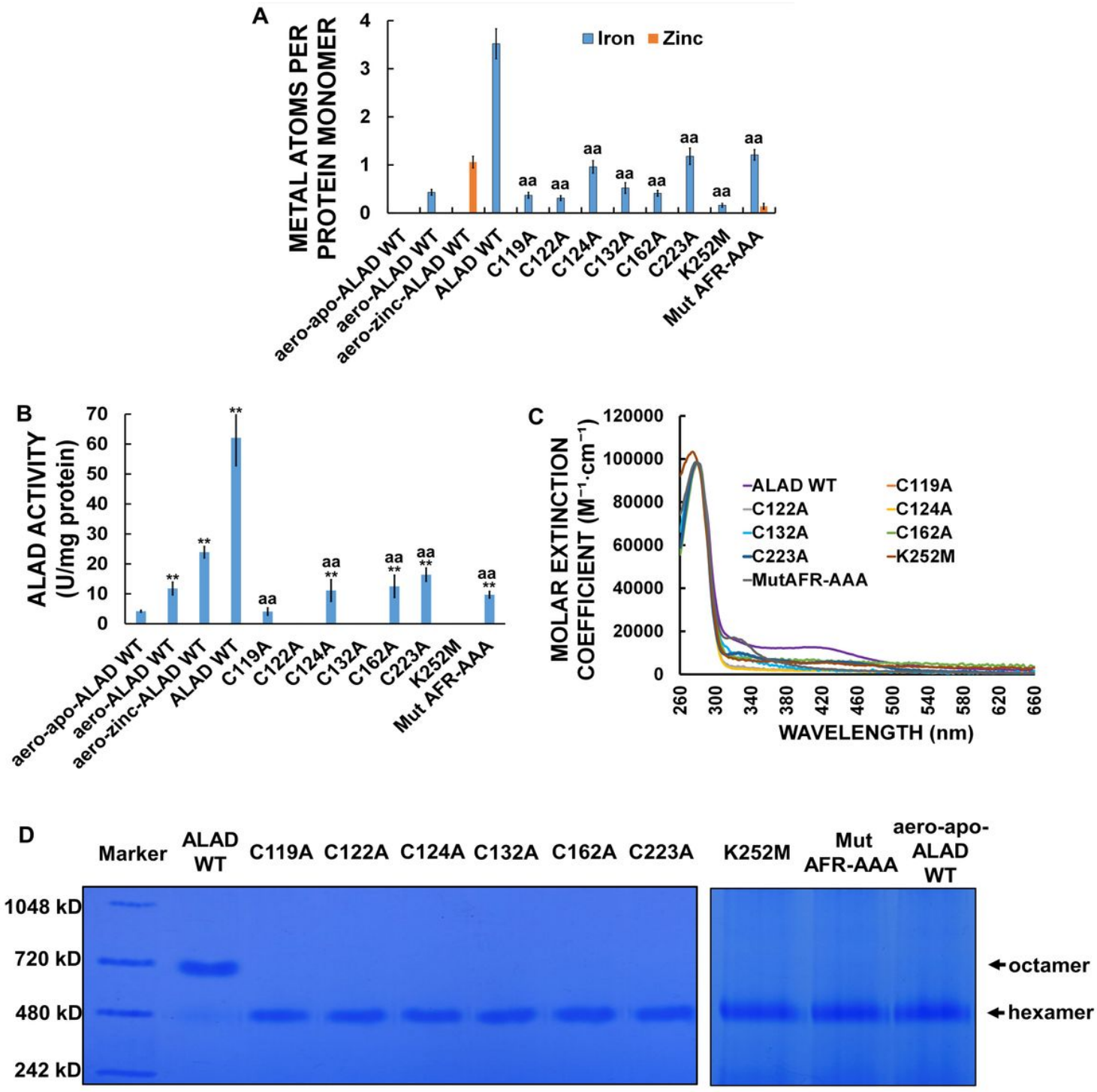

Figure 2

[Fe4S4]-ALAD has significantly higher enzymatic activity than zinc-ALAD, and that cysteines 119, 122, 124, 132, 162, and 223, Lysine 252, and the LYR motif of human ALAD are important for the enzymatic activity of human ALAD that contains a [Fe4S4] cluster in vitro (A) Molar extinction coefficients of C119A, C122A, C124A, C132A, C162A, C223A, K252M and Mut AFR-AAA mutants that were expressed along with the isc operon in E. coli and purified anaerobically. The results indicated that C119, C122, C124, C132, C162, C223, and K252 of human ALAD were important for [Fe4S4] cluster coordination and/or retention, and the AFR motif was important for [Fe4S4] cluster acquisition. (B) ICP-MS analysis and (C) Enzymatic

activity of aero-apo-ALAD WT, aero-Zn-ALAD WT and the wild-type and mutant ALAD proteins expressed along with the isc operon in E. coli and purified anaerobically. Results indicate that the Fe4S42+ cluster was important for the enzymatic activity of human ALAD in vitro. (D) Native gel electrophoresis analysis of wild-type and mutant ALAD proteins expressed along with the isc operon in E. coli and purified anaerobically, and the aero-apo-ALAD WT protein. The results suggest that [Fe4S4] cluster coordination correlated with increased proportions of ALAD homo-octamers. Error bars represent S.D.; ** P<0.01 versus aero-apo-ALAD WT; aa P<0.01 versus ALAD WT.

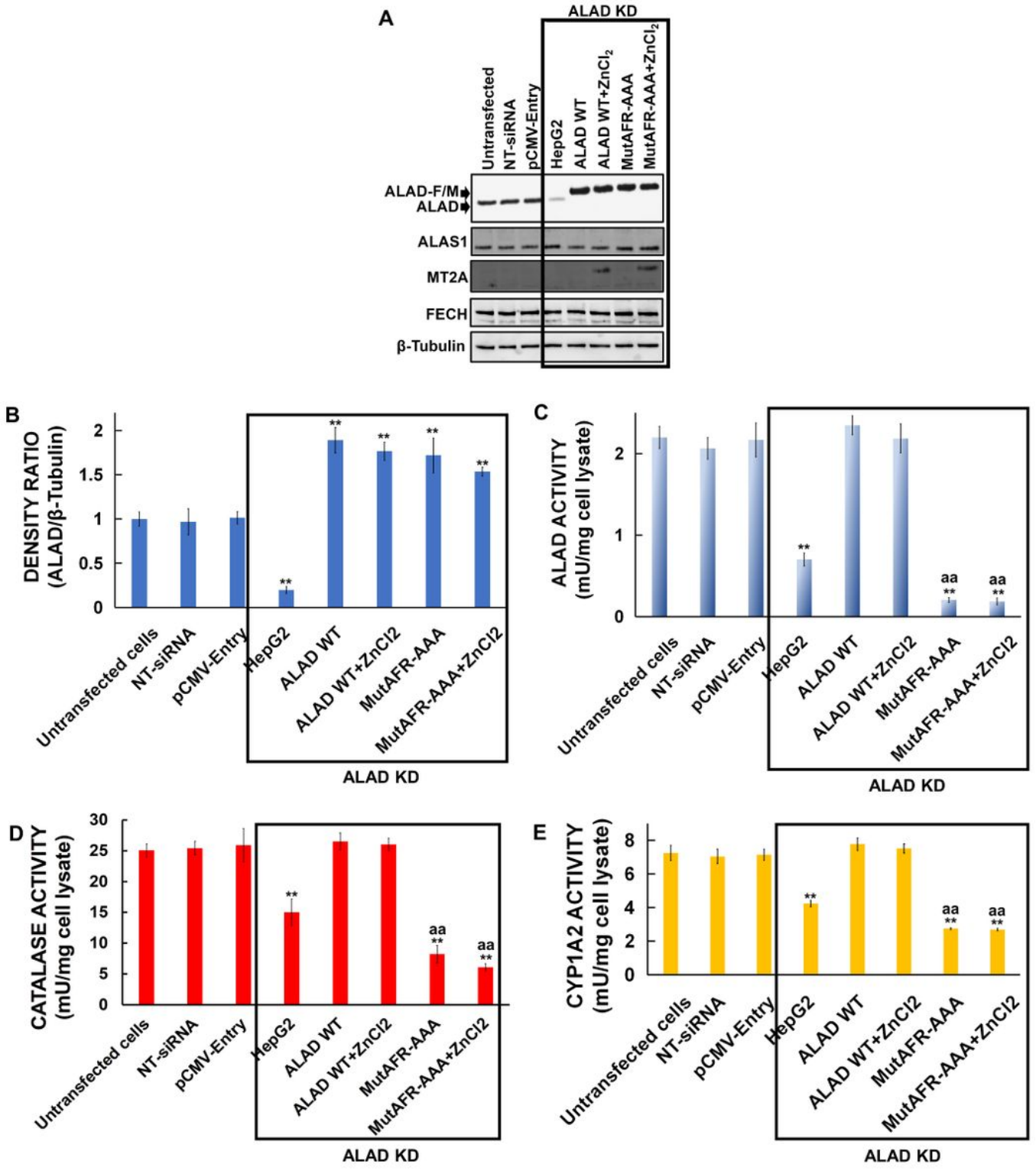

Figure 3

The [Fe4S4] cluster of human ALAD is important for its enzymatic activity and heme biosynthesis in HepG2 cells (A) Western blot analysis of protein levels of endogenous and exogenous ALAD, ALAS1, MT2A and FECH in untransfected HepG2 cells, HepG2 cells transfected with non-targeting siRNA (NT-siRNA) or pCMV-Entry empty vector (pCMV-Entry), ALAD deficient HepG2 cells (ALAD KD), HepG2 cells from the ALAD WT and Mut AFR-AAA groups without or with 100 μM ZnCl2 addition (ALAD WT, ALAD WT+ZnCl2, Mut AFR-AAA or Mut AFR-AAA+ZnCl2, respectively). (B) Densitometry of the ratios between the intensities of ALAD and the corresponding β-Tubulin protein levels. (C) ALAD, (D) catalase, and (E) CYP1A2 activities in lysates of these cells. Error bars represent S.D.; ** P<0.01 versus untransfected HepG2; aa P<0.01 versus HepG2 cells from the ALAD WT group.

Supplementary Files

This is a list of supplementary files associated with this preprint. Click to download.

- ALADmanuscriptSupplementalDocument20200623.docx
- FigureS1.jpg
- FigureS2.jpg
- FigureS3.jpg
- FigureS4.jpg
- FigureS5.jpg
- FigureS6.jpg